Int. J. Electrochem. Sci., 7 **(2012)** 354 - 362

International Journal of
ELECTROCHEMICAL
SCIENCE
www.electrochemsci.org

Graphene Anchored with Nanocrystal Fe_2O_3 with Improved Electrochemical Li-Storage Properties

Shuang-Yu Liu, Jian Xie, Qin Pan, Chun-Yang Wu, Gao-Shao Cao, Tie-Jun Zhu and, Xin-Bing Zhao[*]

Department of Materials Science and Engineering, Zhejiang University, Hangzhou 310027, China
[*]E-mail: zhaoxb@zju.edu.cn

Received: 31 October 2011 / *Accepted:* 10 December 2011 / *Published:* 1 January 2012

Graphene anchored with nanocrystal Fe_2O_3 was synthesized by a two-step solvothermal route. The nanocomposite was characterized by X-ray diffraction (XRD), Raman spectra, X-ray photoelectron spectroscopy (XPS), thermogravimetric analysis (TGA), scanning electron spectroscopy (SEM) and transmission electron microscopy (TEM). It was found that the Fe_2O_3 nano-particles were formed and homogeneously anchored on graphene sheets. The electrochemical properties of the nanocomposite were investigated by galvanostatic cycling. The results showed that the Fe_2O_3/graphere nanocomposite exhibits obviously improved electrochemical properties compared to bare Fe_2O_3 because of the buffering, confining and conducting effects of the introduced grapheme.

Keywords: Fe_2O_3, graphene, nanocomposite, electrochemical properties, anode

1. INTRODUCTION

In the early 1980s, some transition metal oxides, such as CuO [1], Fe_2O_3 [2], and CoO [3] have already been used as cathode in primary batteries. In recent years, these oxides have received a renewed interest since they showed reversible cycling as anodes for Li-ion batteries [4–7]. Among these oxides, Fe_2O_3 is an attractive anode material for lithium ion batteries due to the high theoretical capacity (1005mAh g^{-1}), high abundance of Fe, low cost and low environmental impact [8–10]. However, Fe_2O_3 generally shows a rapid capacity fade because of the large volume changes and agglomerations during the conversion reactions. Great effort has been made to improve the electrochemical properties of Fe_2O_3. A stable cycling could be obtained for Fe_2O_3 by using nanostructured [11, 12], porous [13] and thin-film materials [14] with relieved volume changes.

Dispersing the particles on conducting carbon materials has been proved to be a useful strategy to improve cycling stability of the transition metal oxides due to the effective buffering and conducting effects of carbon materials. In addition, carbon materials also contribute to the overall capacity for the composite. Various forms of carbon, such as amorphous carbon [15], carbon fibers [16], and carbon nanotubes [17] have been suggested as the ideal matrices to disperse Fe_2O_3. Recently, great importance has been attached to another form of carbon, graphene, since reported by Novoselov et al. in 2004 [18]. The intensive researches on tin oxides [19-22], cobalt oxides [23–29], and copper oxides [30, 31] have shown that the cycling stability of these oxides could be greatly improved by loading them onto the graphene.

Graphene, a flat monolayer of sp^2-bonded carbon atoms, is considered as an ideal matrix to disperse nanoparticles due to its advantages such as large specific surface area [32], high electronic conductivity [33], and high mechanical strength [34]. These merits make graphene or graphene-based materials very promising for use as anode materials for Li-ion batteries. In this work, we will investigate the effect of graphene on the electrochemical performance of Fe_2O_3. The Fe_2O_3/graphene (Fe_2O_3/G) nanocomposite was prepared by a two-step solvothermal route. The results showed that the nanocomposite exhibits an obviously improved cycling stability compared with bare Fe_2O_3.

2. EXPERIMENTAL SECTION

2.1 Synthesis of Fe_2O_3/graphene nanocomposite

Graphite oxide (GO, 20 mg), synthesized by a modified Hummer's method [35], was ultrasonically dispersed in a *N*,*N*-dimethylformamide (DMF)/H_2O (10:1 in volume) mixed solvent for 1 h to get graphene oxide followed by adding of 1 mmol $FeSO_4 \cdot 7H_2O$. The above dispersion was then heated at 80 ºC for 3 h. Afterwards, the mixture was sealed into a Teflon-lined stainless steel autoclave and maintained at 180 ºC for 20 h. After it was cooled down to the room temperature, the resulting product was separated by centrifugation, washed with deionized water and ethanol for several times, and dried at 40 ºC under vacuum overnight. For comparison, bare Fe_2O_3 was prepared using the similar procedure without adding GO.

2.2 Materials Characterization

X-ray diffraction (XRD) patterns of the products were collected on a Rigaku D/Max-2550pc powder diffractometer equipped with Cu K_{α} radiation (λ = 1.541 Å). X-ray photoelectron spectroscopy (XPS) analysis was performed on a KRATOS AXIS ULTRA-DLD spectrometer with a monochromatic Al K_{α} radiation ($h\nu$ = 1486.6 eV). The microstructures were observed by field emission scanning electron microscopy (FE-SEM) on a FEI-sirion microscope and transmission electron microscopy (TEM) on a JEM 2100F microscope. Raman spectra were recorded on a Jobin-Yvon Labor Raman HR-800 using 514.5 nm Ar-ion laser. Thermogravimetric analysis (TGA) was performed on a DSCQ1000 instrument from 80 to 800 ºC at a heating rate of 10 ºC min^{-1} in air.

2.3 Electrochemical measurements

The electrochemical properties of the products (Fe_2O_3/G, Fe_2O_3) were evaluated using CR2025-type coin cells. The electrode slurry was prepared by mixing the active material, acetylene black and polyvinylidene fluoride in a weight ratio of 75:15:10 in N-methyl pyrrolidone (NMP) with stirring for 2 h. The working electrodes were made by coating the slurry onto Ni foam current collectors and dried at 100 °C under vacuum overnight. The working electrodes were assembled into half cells in an Ar-filled glove box using Li foil as the counter electrode and polypropylene microporous sheet (Celgard 2300) as the separator. The electrolyte was 1 M $LiPF_6$ dissolved in ethylene carbonate (EC)/dimethyl carbonate (DMC) (1:1, in volume). The cells were galvanostatically charged and discharged between 0.005 and 3 V (vs. Li/Li^+) on a Neware BTS-5V10mA battery cycler (Shenzhen, China). Cyclic voltammetry (CV) measurements were conducted on an Arbin BT2000 system in the voltage range 0.005–3.0 V (vs. Li/Li^+) at 0.1 mV s^{-1}. Electrochemical impedance spectroscopy (EIS) measurements were performed on a CHI660C electrochemistry workstation by applying an ac voltage of 5 mV amplitude in the frequency range from 10 mHz to 100 kHz at de-lithiated states. All of the electrochemical measurements were carried out at room temperature.

3. RESULTS and DISCUSSION

The two-step solvothermal route for Fe_2O_3/G synthesis is schematically illustrated in Fig. 1.

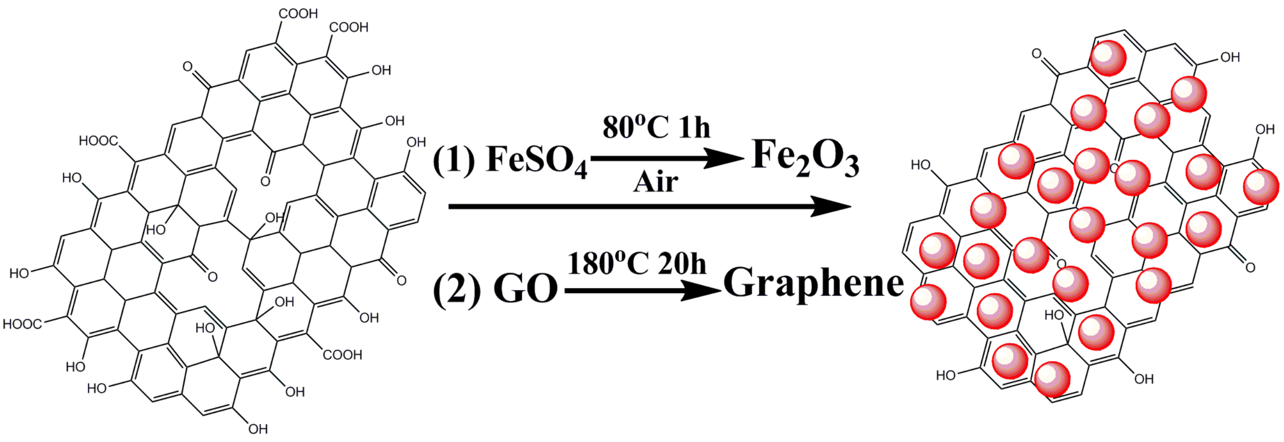

Figure 1. Schematic illustration of the synthetic route of Fe_2O_3/G.

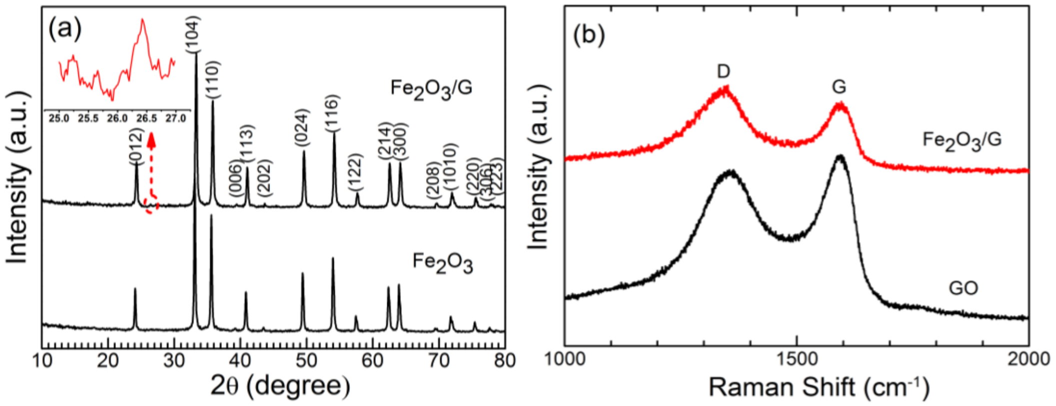

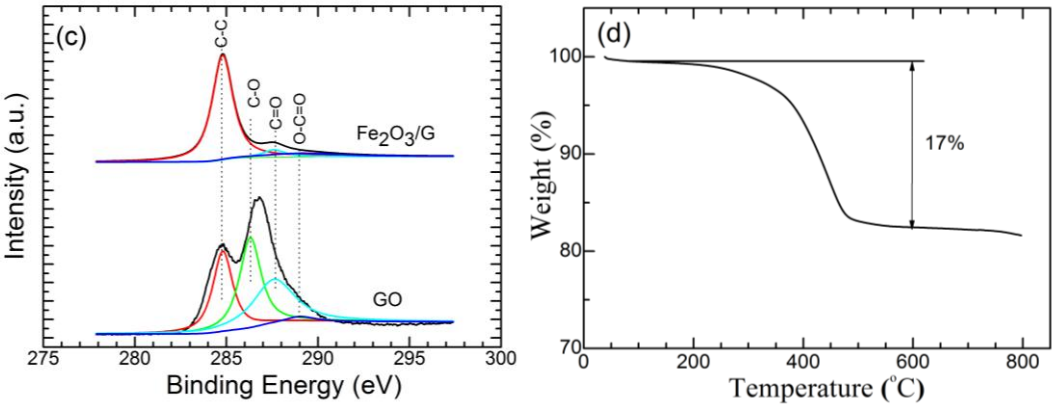

Figure 2. (a) XRD patterns of Fe_2O_3/G and bare Fe_2O_3, (b) Raman spectra of Fe_2O_3/G and GO, (c) C1s XPS of Fe_2O_3/G and GO, and (d) thermogravimetric analysis of Fe_2O_3/G.

In the first step, The Fe^{2+} was undergoes oxidation and hydrolysis in DMF/H_2O to form Fe_2O_3 nanoparticles which are uniformly anchored on the graphene oxide sheets. In the second step, the graphene oxide was reduced to graphene to form the final product Fe_2O_3/G.

Fig. 2(a) shows the XRD patterns of Fe_2O_3/G and Fe_2O_3. The dominant diffraction peaks can be assigned to Fe_2O_3 for both Fe_2O_3/G and Fe_2O_3 (JCPDS No. 33-0664). A hump appears in the range of 26-27° (2□), which originates from graphene as seen in the inset of Fig. 2(a). The small diffraction peak of graphene indicates that the graphene sheets are sufficiently exfoliated by the attached Fe_2O_3 nanoparticles. Fig. 2(b) gives the Raman spectra of GO and Fe_2O_3/G. Both the samples present two bands at 1350 and 1580 cm^{-1}, which correspond to the disordered (D) band and graphitic (G) band of carbon materials [36]. Compared with GO, Fe_2O_3/G exhibits an increased D/G intensity ratio, indicating the conversion from GO to graphene [37].

The conversation of GO into graphene is further proved by XPS analysis as shown in Fig. 2(c). The XPS spectra can be fitted into four peaks, corresponding to carbon atoms in four functional groups: sp^2 carbon (C-C, 284.8 eV), carbon in C-O bonds (286.3 eV), carbonyl carbon (C=O, 287.6 eV) and carboxylate carbon (O-C=O, 290.0 eV) [37].

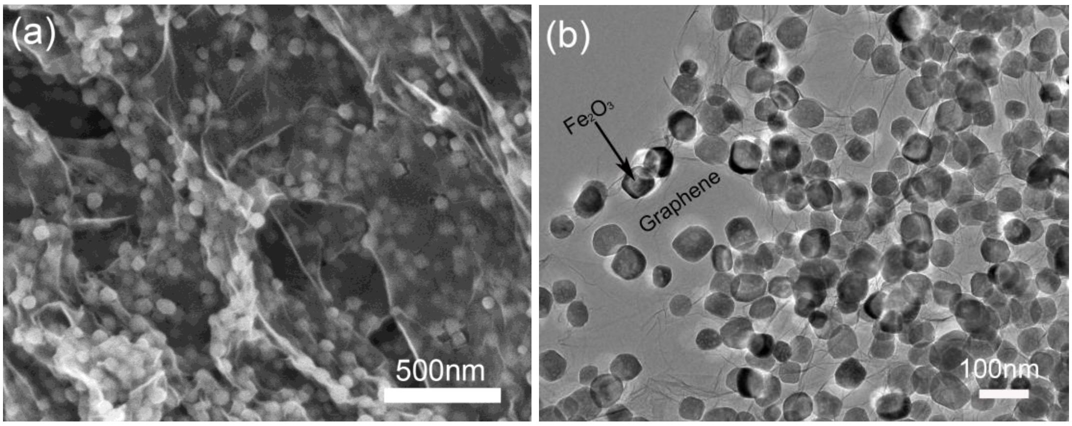

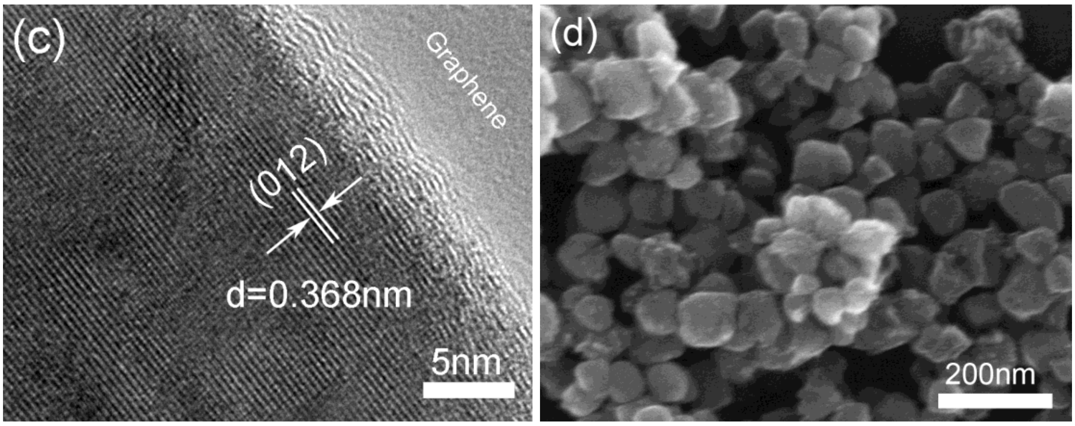

Figure 3. (a) SEM, (b) TEM, (c) HRTEM images of Fe_2O_3/G, and (d) SEM images of bare Fe_2O_3.

After the solvothermal reaction, the peak intensity of carbons in C-O, C=O and O-C=O shows a considerable decrease, confirming that a sufficient reduction of graphene oxide to graphene has occurred. The weight ratio of Fe_2O_3 and graphene was determined by TGA in air as shown in Fig. 2(d). The graphene content is estimated to 17% according to TGA.

Fig. 3(a) shows the SEM images of Fe_2O_3/G synthesized by the solvothermal route at 180 ºC. Through the transparent graphene, it is clear that the Fe_2O_3 nanoparticles are uniformly confined in between the graphene sheets. The nanoparticles show a firm attachment with graphene even though undergone vigorous sonication, implying a strong interaction between graphene and Fe_2O_3. The TEM images in Fig. 3(b) clearly show that the Fe_2O_3 particles with a size of 50–80 nm are homogeneously dispersed by graphene. Fig. 3(c) displays the HRTEM images of an individual Fe_2O_3 particle on graphene. The fringe spacing is measured to be 0.368 nm, corresponding to the interplanar spacing of (012) plane of Fe_2O_3. Without the confinement by graphene, the Fe_2O_3 nanoparticles tend to aggregate as shown in Fig. 3(d).

To study the Li-ion storage properties of Fe_2O_3/G and bare Fe_2O_3, a series of electrochemical measurements were carried out. Fig. 4(a) shows the charge-discharge curves of bare Fe_2O_3 and Fe_2O_3/G for the first three cycles at 50mA g^{-1}. The first charge (Li-extraction) and discharge (Li-insertion) of Fe_2O_3/G are 1270 and 1833 mAh g^{-1}, respectively. The Fe_2O_3/G electrode exhibits a highly reversible cycling evidenced from the almost overlapped charge or discharge curves except for the first cycle. The high reversibility of Fe_2O_3/G could be ascribed to the homogeneous dispersion of the Fe_2O_3 nanoparticles by the highly conductive graphene [38]. In contrast, a large first irreversible capacity and a rapid capacity fade are observed for bare Fe_2O_3. Fig. 4(b) shows the CV plots of Fe_2O_3/G at a scan rate of 0.1 mV s^{-1}. The oxidation and reduction peaks are fixed at around 1.9 V and 0.8 V, respectively, after the first cycle, also indicating the reversible cycling of the electrode.

Fig. 4(c) compares the cycling stability between bare Fe_2O_3 and Fe_2O_3/G at 50mA g^{-1}. Obviously, Fe_2O_3/G shows an improved cycling stability than bare Fe_2O_3. After 30 cycles, Fe_2O_3/G still maintains a discharge capacity of 1043 mAh g^{-1}, while for bare Fe_2O_3, its capacity drops rapidly to 89 mAh g^{-1} after the same cycles. The cycling performance of the Fe_2O_3/G electrode at 300 mA g^{-1} was also evaluated as shown in Fig. 4(d). After 50 cycles, Fe_2O_3/G still retains a capacity of 496 mAh

g^{-1}. The enhancement in cycling stability could be attributed to the introduction of graphene that acts both as a buffer to accommodate the volume changes and as a separator to prevent the Fe_2O_3 nanoparticles from aggregating.

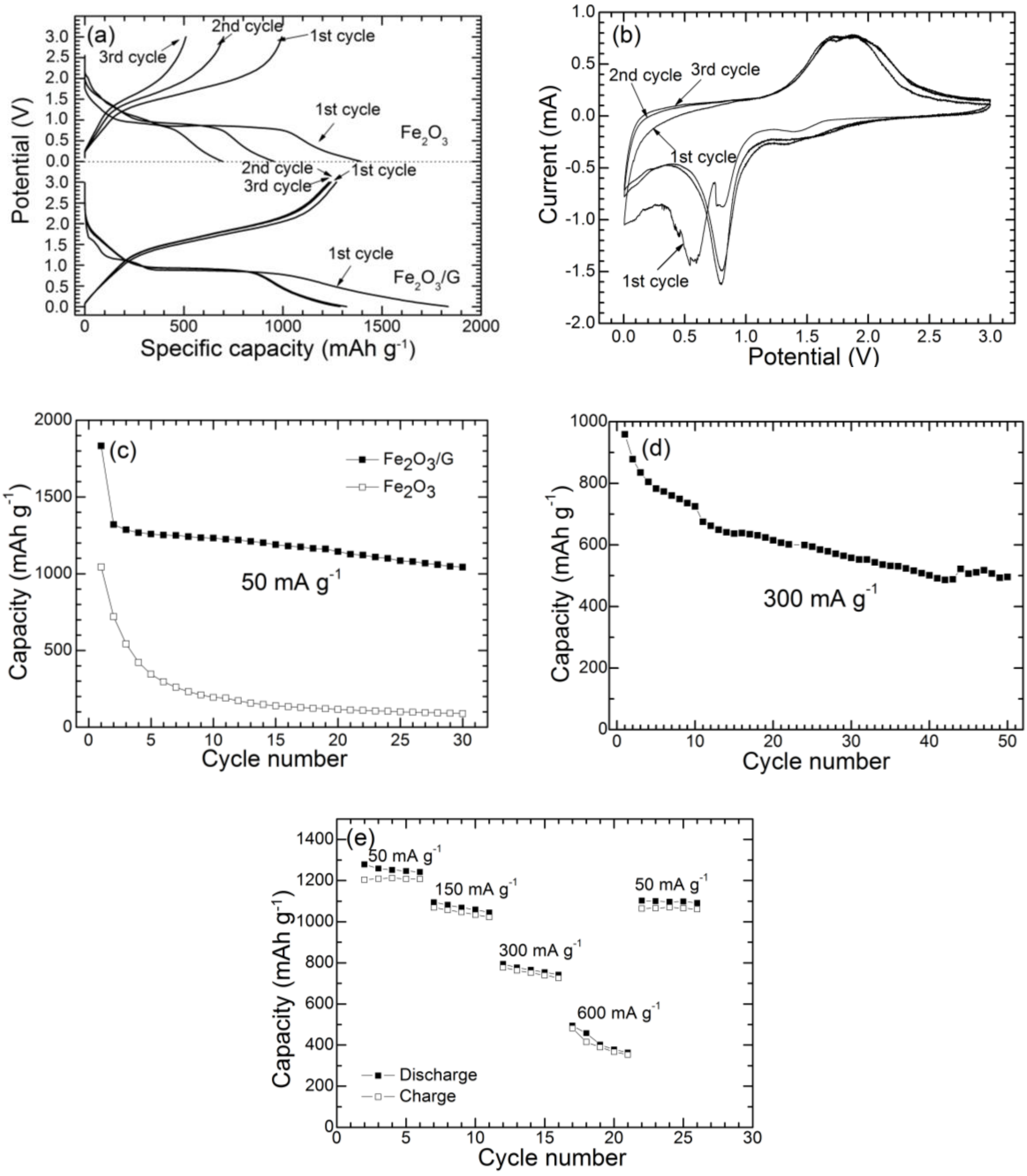

Figure 4. Electrochemical properties of the solvothermal products: (a) charge-discharge curves of Fe_2O_3/G and bare Fe_2O_3 at 50 mA g^{-1}, (b) CV plots of Fe_2O_3/G at 0.1 mV s^{-1}, (c) comparison of cycling stability between Fe_2O_3/G and bare Fe_2O_3 at 50 mA g^{-1}, (d) cycling stability of Fe_2O_3/G at 300 mA g^{-1}, and (e) rate capability of Fe_2O_3/G.

Fig. 4e shows the rate capability of Fe_2O_3/G. Note that Fe_2O_3/G exhibits a good rate capability. After being cycled at high rates, the capacity can be well recovered once the current is shifted to a low value, indicating a good reversibility for Fe_2O_3/G. The good rate capability comes mainly from the two factors: first, the highly conductive graphene supplies two-dimensional (2D) conducting channels for the Fe_2O_3 nanoparticles; second, the homogeneous dispersion of Fe_2O_3 nanoparticles by graphene leads to a good wetting of the active material by the electrolyte and thus facilitates the rapid Li-ion diffusion at the electrode/electrolyte interface. Furthermore, the small-sized Fe_2O_3 is also favorable for rapid Li-ion solid phase diffusion when it is effectively confined by graphene.

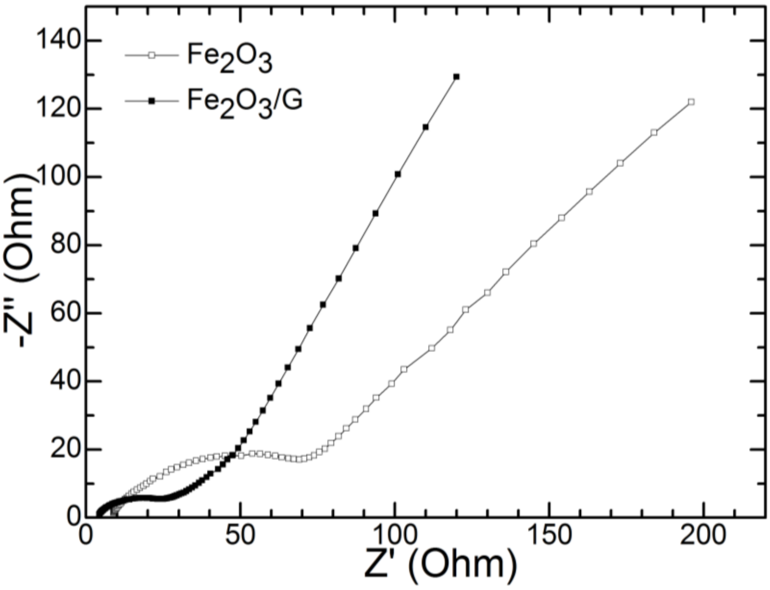

Figure 5. Nyquist plots of Fe_2O_3/G and bare Fe_2O_3 electrodes after 10 cycles

EIS measurements were carried out to understand the effect of graphene on the electrochemical behaviors of Fe_2O_3. Fig.5 gives the Nyquist plots of the Fe_2O_3 and Fe_2O_3/G composites after 10 charge-discharge cycles. The plots are composed of two partially overlapped semicircles at high- and medium-frequency ranges and a sloping line at the low frequency range. The high-frequency semicircle corresponds to the solid electrolyte interface (SEI) layer resistance R_{SEI}; the middle-frequency semicircle is related to the charge transfer resistance R_{ct}; the sloping line at the low frequency is associated with the Li-ion solid phase diffusion in the bulk electrode. The Fe_2O_3/G electrode shows smaller R_{SEI} and R_{ct} than the bare Fe_2O_3 electrode. The better wetting the active material and refrained particles aggregation are responsible for the low R_{ct} value for Fe_2O_3/G. The stabilization of the electrode by confining the active particles between the graphene sheets is considered to account for its low R_{SEI} value. A lower R_{ct} for Fe_2O_3/G can explain its good cycling stability and rate capability. In addition, a low R_{SEI} value is also beneficial for the reversible cycling of the electrode. As a result, the EIS measurements agree well with the different electrochemical behaviors of Fe_2O_3 with and without graphene.

4. CONCLUSIONS

Fe_2O_3-graphene nanocomposites have been synthesized by a two-step solution route. The nanoparticles with an average size of 50‒80 nm are uniformly anchored on graphene. The nanocomposite shows improved electrochemical properties compared to the bare oxide. The improvement in electrochemical performance is attributed to the flexible graphene that not only buffers the volume changes but also refrains the aggregation of nanoparticles. The introduced graphene also offers a 2D conductive network and increases the wetting of the active material, also contributing to enhanced electrochemical performance.

ACKNOWLEDGEMENTS
This work was supported by Zijin Program of Zhejiang University, China, the Fundamental Research Funds for the Central Universities (No. 2010QNA4003), the Ph.D. Programs Foundation of Ministry of Education of China (No. 20100101120024), the Foundation of Education Office of Zhejiang Province (No. Y201016484), the Qianjiang Talents Project of Science Technology Department of Zhejiang Province (2011R10021), and the National Natural Science Foundation of China (No. 51101139).

References

1. T. Iijima, Y. Toyoguchi, J. Nishimura, and H. Ogawa, *J. Power Sources* 5 (1980) 99.
2. M. M. Thackeray and J. Coetzer, *Mater. Res. Bull.* 16 (1981) 591.
3. M. M. Thackeray, S. D. Baker, and J. Coetzer, *Mater. Res. Bull.* 1 (1982) 405.
4. P. Poizot, S. Laruelle, S. Grugeon, L. Dupont, and J. M. Tarascon, *Nature* 407 (2000) 496.
5. A.Débart, L. Dupont, P. Poizot, J. B. Leriche, and J. M. Tarascon, *J. Electrochem. Soc.* 148 (2001) A1266.
6. S. Grugeon, S. Laruelle, R. Herrera-Urbina, L. Dupont, P. Poizot, and J. M. Tarascona, *J. Electrochem. Soc*. 148 (2001) A285.
7. F. Badway, I. Plitz, S. Grugeon, S. Laruelle, M. Dollé, A. S. Gozdz, and J. M. Tarascon, *Electrochem. Solid State Lett.* 5 (2002) A115.
8. H. Liu, G. Wang, J. Park, J. Wang, H. Liu, and C. Zhang, *Electrochim. Acta.* 54 (2009) 1733.
9. L. C. Yang, Q. S. Gao, Y. H. Zhang, Y. Tang, and Y. P. Wu, *Electrochem. Commun*. 10 (2008) 118.
10. H. Liu, D. Wexler, and G. Wang, *J. Alloys Compd*. 487 (2009) L24.
11. Y. N. NuLi, R. Zeng, P. Zhang, Z. P. Guo, and H. K. Liu, *J. Power Sources* 184 (2008) 456.
12. J. P. Liu, Y. Y. Li, H. J. Fan, Z. H. Zhu, J. Jiang, R. M. Ding, Y. Y. Hu, and X. T. Huang, *Chem. Mater*. 22 (2010) 212.
13. B. Sun, J. Horvat, H. S. Kim, W. S. Kim, J. Ahn, and G. X. Wang, *J. Phys. Chem. C* 114 (2010) 18753.
14. L. Wang, H. W. Xu, P. C. Chen, D. W. Zhang, C. X. Ding, and C. H. Chen, *J. Power Source* 193 (2009) 846.
15. M. G. B. Sassin, A. N. Mansour, K. A. Pettigrew, D. R. Rolison, and J. W. Long, *ACS Nano* 8 (2010) 4505.
16. M. S. Wu, Y. H. Ou, and Y. P. Lin, *Electrochim. Acta* 55 (2010) 3240.
17. S. L. Chou, J. Z. Wang, Z. X. Chen, H. K. Liu, and S. X. Dou, *Nanotechnology* 22 (2011) 265401.
18. K. S. Novoselov, A. K. Geim, S. V. Morozov, D. Jiang, Y. Zhang, S. V. Dubonos, I. V. Grigorieva, and A.A. Firsov, *Science* 306 (2004) 666.

19. D. H. Wang, R. Kou, D. W. Choi, Z. G. Yang, Z. M. Nie, J. Li, L. V. Saraf, D. H. Hu, J. H. Zhang, G. L. Graff, J. Liu, M. A. Pope, and I. A. Aksay, *ACS Nano* 3 (2010) 1587.
20. S. M. Paek, E. J. Yoo, and I. Honma, *Nano Lett.* 9 (2009) 72.
21. J. Yao, X. P. Shen, B. Wang, H. K. Liu, and G. X. Wang, *Electrochem. Commun*. 11 (2009) 1849.
22. L. S. Zhang, L. Y. Jiang, H. J. Yan, W. D. Wang, W. Wang, W. G. Song, Y. G. Guo, and L. J. Wan, *J. Mater. Chem*. 20 (2010) 5462.
23. S. Q. Chen and Y. Wang, *J. Mater. Chem.* 20 (2010) 9735.
24. Z. S. Wu, W. C. Ren, L. Wen, L. B. Gao, J. P. Zhao, Z. P. Chen, G. M. Zhou, F. Li, and H. M. Cheng, *ACS Nano* 4 (2010) 3187.
25. S. B. Yang, X. L. Feng, S. Ivanovici, and K. Müllen, *Angew. Chem. Int. Ed.* 49 (2010) 8408.
26. H. Kim, D.H. Seo, S.W. Kim, J. Kim, and K. Kang, *Carbon* 49 (2011) 326.
27. B. J. Li, H .Q. Cao, J. Shao, G. Q. Li, M. Z. Qu, and G. Yin, *Inorg. Chem.* 50 (2011) 1628.
28. J. X. Zhu, Y. K. Sharma, Z. Y. Zheng, X. J. Zhang, M. Srinivasan, S. Mhaisalkar, H. Zhang, H. H. Hng, and Q. Y. Yan, *J. Phys. Chem. C*. 115 (2011) 8400.
29. J. X. Zhu, T. Zhu, X. Z. Zhou, Y. Y. Zhang, X. W. Lou, X. D. Chen, H. Zhang, H. H. Hng, and Q. Y. Yan, *Nanoscale* 3 (2011)1084.
30. B. Wang, X. L. Wu, C. Y. Shu, Y. G. Guo, and C. R. Wang, *J. Mater. Chem.* 20 (2010) 10661.
31. Y. J. Mai, X. L. Wang, J. Y. Xiang, Y. Q. Qiao, D. Zhang, C. D. Gu, and J. P. Tu, *Electrochim. Acta*. 56 (2011) 2306.
32. M. D. Stoller, S. Park, Y. W. Zhu, J. H. An, and R. S. Ruoff, *Nano Lett*. 8 (2008) 3498.
33. S. Park, J. H. An, I. W. Jung, R. D. Piner, S. J. An, X. S. Li, A. Velamakanni, and R. S. Ruoff, *Nano Lett.* 9 (2009) 1593.
34. C. Lee, X. D. Wei, J. W. Kysar, and J. Hone, *Science* 321 (2008) 385.
35. W. S. Hummers and R. E.Offeman, *J. Am. Chem. Soc.* 80 (1958) 1339.
36. F. Tuinstra, J. L. Koenig, *J. Chem. Phys*. 53 (1970) 1126.
37. S. Stankovich, D. A. Dikin, R. D. Piner, K. A. Kohlhaas, A. Kleinhammes, Y. Y. Jia, Y. Wu, S. T. Nguyen, R. S. Ruoff, *Carbon* 45 (2007) 1558.
38. S. Park, J. H. An, I. W. Jung, R. D. Piner, S. J. An, X. S. Li, A. Velamakanni, R. S. Ruoff, *Nano Lett*. 9 (2009) 1593.